

# Radiation characteristics and detection capability model and analysis of small target in infrared radiation system

LI LIN<sup>1,\*</sup>, JIACHENG CHEN<sup>2</sup>, QIANG MENG<sup>2</sup>

<sup>1</sup>College of Art & Design, Chongqing Jiaotong University, Chongqing, 400074, P. R. China

<sup>2</sup>College of Electromechanical and Automotive Engineering, Chongqing Jiaotong University, Chongqing, 400074, P. R. China

The target infrared radiation brightness is a key index for the infrared radiation system to obtain target characteristics and recognize the target. This paper proposes a calculation method to accurately evaluate the detection capability of the infrared radiation system and establishes the calibration calculation model of the infrared radiation system using multiple integration times. The calculation function of the target radiation brightness is constructed according to the principle that the total energy of the target in the infrared detector diffusion imaging is constant, and considering the factors such as atmospheric jitter, optical system diffraction and imaging aberration. Based on this, combined with the dispersion phenomenon of the test environment, the calculation model of the detection distance of the system is deduced. Based on the test platform with known parameters, the correlation between the detection distance and the target radiation brightness and the rationality of the detection distance calculation model established in this paper are calculated and analyzed. The obtained results provide a reference for the reliable detection of the infrared system under the condition of long-range in complex environments.

(Received December 12, 2022; accepted April 7, 2023)

*Keywords:* Infrared detector, Target radiation brightness, Dispersion coefficient, Detection distance

## 1. Introduction

The infrared radiation system is used to measure the infrared radiation characteristics including the target radiation brightness, the temperature, the radiation intensity, and other information, and can provide scientific data for the evaluation of capabilities such as target stealth effect, and detection and recognition of targets [1-2]. Currently, the research direction of the infrared system has two aspects. First, focusing on the center position and size of the target to find and accurately locate the target as early as possible [3-5], and achieve target detection and tracking. Second, focus on the radiation brightness of the target, which can be obtained according to the gray scale of the target imaging pixel. Tiejing Qiao et al. [6] studied the method of measuring the opposite target based on the infrared radiation characteristic system and proposed a reliable area analysis method and radiation brightness calculation method. Guoqiang Wang et al. [7] established a ground-based measurement simulation model for space target temperature and equivalent radiation area using the infrared system characteristics, the target radiation characteristics and the infrared radiation atmospheric transmission characteristics. Chengming Sun et al. [8] established a mathematical model for the infrared spectral characteristics and imaging characteristics of space targets using the bidirectional reflection distribution function, and presented the calculation formula for the energy distribution of targets at the entrance pupil of the detector and on the image plane. Hongyuan Wang et al. [9] modelled the infrared dynamic radiation characteristics of

space targets, established a physical model for the radiation characteristics of space targets according to the characteristics of targets and backgrounds, and established a mathematical model for the infrared reflection characteristics of targets using the bidirectional reflection distribution function. Jiahao Xie et al. [10] analyzed the detection capability of the air space infrared detection system for the unmanned aerial vehicle (UAV) swarm and established a noise equivalent flux density point target detection range model based on the dispersion coefficient. However, the target detected in this paper is a small UAV. Moreover, the infrared radiation system was used for measurement, when the target was close to the measurement system, the imaging range of the target on the detector surface was large and when the target was far away from the measurement system, the ideal imaging range of the target on the detector surface was smaller than the size of a single pixel. It is inappropriate to regard such small targets as area source or point source targets, and the processing method of area source or point source targets will introduce large measurement errors [11]. At the same time, in practical engineering applications, when the target is far from the measurement system, its ideal imaging range occupies multiple pixels on the detector surface. When the target imaging is small, the imaging energy will be dispersed to multiple pixels and form a speckle due to various factors including atmospheric disturbance and optical system aberration or diffraction. The characteristics of this speckle are that the gray value of the entire infrared image is inconsistent, and the edge of the infrared image is fuzzy [12]. Therefore, the UAV target is treated as a small

target according to the characteristics of the UAV target infrared image collected by the area source target or point source target to obtain accurate infrared radiation energy, and the correlation model between the target incident radiance and the detector pixel output gray is established. The infrared radiation system must be calibrated before the measurement to obtain the response and offset of the infrared detector in the system, and provide a reference for the quantitative relationship between the target incident radiance and the detector pixel output gray.

## 2. Infrared radiation measurement calibration model

Calibration is an important index to test the radiation measurement performance of the infrared system, and it determines the reliability and effectiveness of the system in the measurement process. The basic principle of calibration is to use the known blackbody as the radiation source to obtain the output signal of the system under different radiation illuminations to establish the relationship between the entrance pupil radiation and the output of the system. Multiple integration times are required for calibration to improve calibration accuracy and efficiency. Accurate calibration can expand the dynamic range of the measurement system and combine the characteristics of the target flight. This paper adopts the uniform large-area source blackbody calibration method with multiple integration times.

The principle diagram of the uniform large-area source blackbody method is shown in Fig. 1. The calibration process is as follows. A uniform large-area source blackbody is placed at the entrance pupil of the infrared radiation system. The effective area of the large-area source blackbody should completely cover the pupil of the infrared radiation system, and use the blackbody as a standard Lambert body to critically illuminate the radiation characteristic measurement system [13]. The uniform large-area source blackbody method can effectively eliminate the influence of the external environment in the calibration process and the influence of the transmissivity. It can realize the calibration of all pixels and can achieve high calibration accuracy.

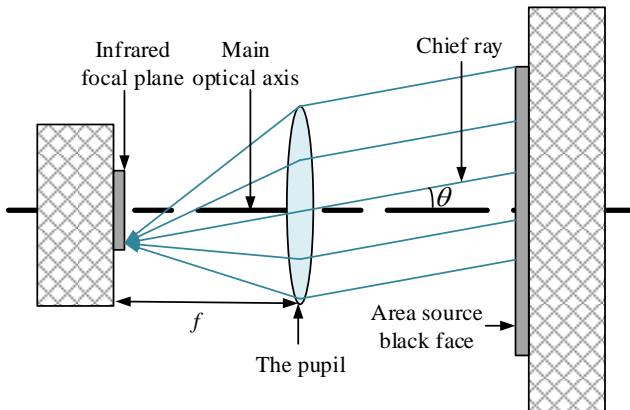


Fig. 1. Schematic diagram of the principle of the uniform large area source blackbody method

In Fig. 1, it is assumed that the intersection angle between the chief ray and the main optical axis is  $\theta$ , and the solid angle of a single pixel in the infrared detector is:

$$\Omega = A_d \cdot \cos^3 \theta / f^2 \quad (1)$$

where,  $A_d$  is the area of a single pixel in the infrared detector, and  $f$  is the focal length of the optical system.

The radiation flux of a large-area source blackbody incident on the infrared detector pixel is expressed as:

$$\omega = \frac{1}{4} \pi \cdot \xi \cdot \Phi(T_b) \cdot \tau_1 \cdot A_d \cdot \cos^4 \theta \cdot \left(\frac{d}{f}\right)^2 \quad (2)$$

where,  $\xi$  and  $T_b$  are the emissivity and the temperature of the blackbody, respectively,  $\tau_1$  and  $d$  are the transmissivity and the aperture of the optical system,

respectively, and  $\kappa_t = \frac{1}{4} \pi \cdot \xi \cdot \tau_1 \cdot A_d \cdot \left(\frac{d}{f}\right)^2$ .

The response coefficient of the infrared detector pixel to incident radiation flux under unit integration time is  $K_{xy}$ ,

$K_{xy} = K'_{xy} / \kappa_t$ ,  $K'_{xy}$  is the response of the infrared detector pixel to incident radiation flux in unit integration time, and  $\Phi(T_b)$  is calibration blackbody radiation brightness, which is expressed as:

$$\Phi(T_b) = \frac{\xi}{\pi} \int_{\lambda_1}^{\lambda_2} W(\lambda, T_b) d\lambda \quad (3)$$

where,  $\lambda_1 \sim \lambda_2$  is the range of the working band of the infrared detector, and  $W(\lambda, T_b)$  is the ideal blackbody radiation brightness, which can be calculated by Planck's formula [14].

The infrared radiation system studied in this paper uses a cooled infrared focal plane array as an infrared imaging detector. The relationship between the gray response and the radiation brightness is expressed as follows:

$$\begin{aligned} G_{xy} &= K'_{xy} \cdot \Phi(T_b) + K_{xy} \cdot \Phi^s + \bar{G}_{xy}^d \\ &= K'_{xy} \cdot \Phi(T_b) + \bar{G}_{xy} \end{aligned} \quad (4)$$

where,  $G_{xy}$  is the output gray value of the infrared detector,  $\bar{G}_{xy} = K_{xy} \cdot \Phi^s + \bar{G}_{xy}^d$ ,  $\bar{G}_{xy}$  is the initial offset response when target infrared radiation brightness enters the infrared detector,  $\bar{G}_{xy}^s = K_{xy} \cdot \Phi^s$ ,  $\bar{G}_{xy}^s$  is the gray response caused by the external stray radiation,  $\Phi^s$  is the stray radiation brightness of the infrared radiation system

caused by external factors, and  $\bar{G}_{xy}^d$  is the gray response caused by the internal factors such as the dark current of the infrared detector [15].

According to the relationship that the integration time of the detector in the linear response range of the infrared radiation system is proportional to the output gray of the system, and multiple integration time ranges set by the system, the calibration calculation model of the infrared radiation system is defined as:

$$G'_{xy} = t \cdot [K'_{xy} \cdot \Phi(T_b) + K_{xy} \cdot \Phi^s] + \bar{G}_{xy}^d \quad (5)$$

### 3. Modeling of target radiation characteristics and detection capability of an infrared radiation system

#### 3.1. Target radiation characteristics of an infrared radiation system

In the process of detecting space targets by the infrared radiation system, the actual imaging of target energy on the detection surface of the infrared detector will occupy multiple pixels after dispersion due to different factors such as atmospheric jitter, optical system diffraction and imaging aberration. At this time, the dispersion of target energy will affect the accuracy of the system measurement. To accurately calculate the target radiation energy, it is necessary to obtain all the energy of the target reaching the infrared detector and eliminate the influence of energy dispersion on the measurement accuracy of the system. Fig. 2 shows the imaging diagram of the target in the infrared detector.

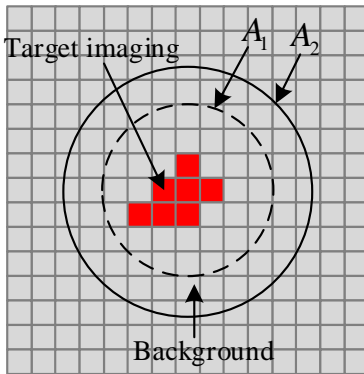


Fig. 2. Schematic diagram of the target in the infrared detector (color online)

In Fig. 2, the target imaging range area is  $A_1$ , which includes the entire target speckle and a small part of the background, called the "target area". There are  $m_1$  pixels in total, including all the pixels containing the target imaging energy and a part of the background imaging pixels. Hence, all the energy of the target imaging is

within the area  $A_1$ . Since the area  $A_1$  includes target energy and background energy, the influence of background must be excluded to accurately obtain target energy. Another area  $A_2$  is selected at the periphery of the area  $A_1$ . The areas between the areas  $A_1$  and  $A_2$  only contain the background, which is called the "background area". The number of pixels in the area is  $m_2 - m_1$ . Since the size of a single pixel of the infrared detector is  $A_d$ , the total background area is  $(m_2 - m_1) \cdot A_d$ . The average gray value of the background area is calculated as:

$$\bar{G}_b = \frac{\sum_{j=1}^{m_2-m_1} G_j}{m_2 - m_1} \quad (6)$$

where,  $G_j, j = 1, 2, \dots, m_2 - m_1$  is the gray value of the background area pixel.

In practical application, the target is far from the infrared radiation system, and the atmosphere between the target and the measurement system will affect the measurement accuracy, which must be considered. Assuming that the atmospheric transmittance is  $\tau_2$  and the atmospheric path radiation brightness is  $\Phi(L_{ts})$ , the average gray value of the background area is defined as:

$$\bar{G}_b = \tau_2 \cdot K''_{xy} \cdot \Phi(T_B) + K''_{xy} \cdot \Phi(L_{ts}) + \bar{G}_{xy} \quad (7)$$

where,  $K''_{xy}$  is the response of the infrared detector pixel to target radiation brightness that can be obtained by blackbody calibration of area source [16], and  $\Phi(T_B)$  is the background radiation brightness.

According to Formula (7), the background radiation brightness is calculated as:

$$\Phi(T_B) = \frac{\bar{G}_b - K''_{xy} \cdot \Phi(L_{ts}) - \bar{G}_{xy}}{\tau_2 \cdot K''_{xy}} \quad (8)$$

Assuming that the ideal imaging size of the target is  $\tilde{A}_t$ , according to the geometric optical object image relationship, Formula (9) is obtained:

$$\tilde{A}_t = N^2 \cdot A_t = \left( \frac{f}{L_1 - f} \right)^2 \cdot A_t \quad (9)$$

where,  $N$  is the magnification of the measuring system,  $N = \frac{L_2}{L_1}$ , according to  $\frac{1}{L_1} + \frac{1}{L_2} = \frac{1}{f}$ , so  $N = \frac{f}{L_1 - f}$ ,  $L_1$  and  $L_2$  are the object distance and the image distance,

respectively, and  $A_t$  is the projected area of the target on the image plane of the infrared detector, which can be obtained from the size and attitude of the target.

The total gray level of all pixels in the area  $A_t$  is  $G_{Al} = \sum_{j=1}^{m_1} G_j$ . The total gray value of background radiation is expressed as:

$$G_b = \frac{(m_1 \cdot A_d - N^2 \cdot A_t)}{A_d} \cdot (\tau_2 \cdot K_{xy}'' \cdot \Phi(T_B) + K_{xy}'' \cdot \Phi(L_{ts}) + \bar{G}_{xy}) \quad (10)$$

The total gray value of target radiation is expressed:

$$G_{Alt} = \frac{N^2 \cdot A_t}{A_d} \cdot [\tau_2 \cdot K_{xy}'' \cdot \Phi(T_t) + K_{xy}'' \cdot \Phi(L_{ts}) + K_{xy}'' \cdot \Phi^s + \bar{G}_{xy}^d] \quad (11)$$

According to Formula (11), the gray value of target radiation is related to the focal length, the transmittance and the aperture of the optical system, the area of a single pixel in the infrared detector, the size and attitude of the space target, the atmospheric transmittance, the response coefficient of the infrared detector, and the distance between the target and the detection system.

Since the total gray level is equal in area  $A_t$ ,

$G_{Al} = G_b + G_{Alt}$ , then:

$$\sum_{j=1}^{m_1} G_j = \frac{(m_1 \cdot A_d - N^2 \cdot A_t)}{A_d} \cdot [\tau_2 \cdot K_{xy}'' \cdot \Phi(T_B) + K_{xy}'' \cdot \Phi(L_{ts}) + \bar{G}_{xy}] + \frac{N^2 \cdot A_t}{A_d} \cdot [\tau_2 \cdot K_{xy}'' \cdot \Phi(T_t) + K_{xy}'' \cdot \Phi(L_{ts}) + \bar{G}_{xy}] \quad (12)$$

Therefore, the target radiation brightness is defined as:

$$\Phi(T_t) = \frac{\sum_{j=1}^{m_1} G_j - m_1 \cdot [K_{xy}'' \cdot \Phi(L_{ts}) + \bar{G}_{xy}]}{\tau_2 \cdot K_{xy}'' \cdot N^2 \cdot A_t / A_d} - \frac{m_1 \cdot A_d - N^2 \cdot A_t}{N^2 \cdot A_t} \cdot \frac{\bar{G}_b - K_{xy}'' \cdot \Phi(L_{ts}) - \bar{G}_{xy}}{\tau_2 \cdot K_{xy}''} \quad (13)$$

### 3.2. Modeling of detection capability of an infrared radiation system

For reliable detection of the system, the optical system used by the actual infrared radiation system in the detection process of space targets is not an ideal optical system, that is, the target imaging is not an ideal geometric point, but a diffused image spot. Therefore, the two-dimensional Gaussian point spread function is used to approximate the description. The amplitude response of any position on the image plane of the infrared detector is expressed as:

$$F(X, Y) = \frac{1}{2\pi\sigma^2} \exp\left[-\frac{(X - X_i)^2 + (Y - Y_i)^2}{2\sigma^2}\right] \quad (14)$$

where,  $(X_i, Y_i)$  is the position coordinate of the image plane of the infrared detector, and  $\sigma$  is the standard deviation, which is related to the focal length of the optical lens and the working band of the infrared detector. The dispersion phenomenon of target imaging points is expressed by the dispersion coefficient.

$$\mu = \sigma_t^2 / \sigma_{tc}^2 \quad (15)$$

where,  $\sigma_t$  is the root mean square (RMS) value of the angle between the target diameter and the detection surface of the infrared detector, and  $\sigma_{tc}$  is the RMS value of the angle between the diffuse spot of the actual imaging point of the target and the measurement system [17-18]. Both RMS values are expressed as:

$$\sigma_t = \frac{1}{2\sqrt{3}} \cdot \frac{\sqrt{A_t}}{R} \cdot \frac{180 \times 3600}{\pi}, \quad \sigma_{tc} = \sqrt{\sigma_t^2 + \sum_{k=1}^6 \sigma_k^2};$$

where  $R$  is the detection distance and  $\sigma_k (k=1, 2, \dots, 6)$  is the RMS value of dispersion caused by the infrared detector and atmosphere. According to Formula (15), the dispersion coefficient decreases with the increase in the detection distance, which is proportional to the projected area of the target. Therefore, the influence of the variation of the dispersion coefficient should be considered while studying the detection distance model of the infrared system to the target.

When the infrared radiation received by the infrared radiation system can just meet the threshold signal-to-noise ratio (SNR) of the system, the distance is called the detection distance of the system [19-20]. The radiation received by the target pixel consists of target radiation, background radiation and path radiation. The radiation received by the background pixel consists of background radiation and path radiation. The radiation received by the background pixel is affected by the atmospheric environment and background radiation characteristics [21]. Its model expression is:

$$P_b = \frac{A_0}{R^2} A_t \tau_1 \tau_2 \Phi(T_B) + \frac{A_0}{R^2} A_t \tau_1 \Phi(L_{ts}) \quad (16)$$

where,  $A_0$  is the entrance pupil area of the optical system, and  $A_0 = \pi d^2 / 4$ .

The radiation power received by the target pixel is expressed as:

$$P_t = \frac{A_0}{R^2} A_t \mu \tau_1 \tau_2 \Phi(T_t) + \frac{A_0}{R^2} A_t \tau_1 \Phi(L_{ts}) \quad (17)$$

According to the difference of radiation power between the target and the background pixels, the irradiance difference of the system pupil can be calculated as:

$$\Delta\Phi = \frac{P_t - P_b}{A_0 \tau_1} = \frac{[\mu\Phi(T_t) - \Phi(T_B)] \cdot A_t \tau_2}{R^2} \quad (18)$$

The equivalent noise amplitude of the system is expressed as:

$$NEFD = \frac{\sqrt{A'_d \Delta f}}{A_0 \tau_1 D^*} \quad (19)$$

where,  $A'_d$  is the effective area of the infrared detector,  $\Delta f$  is the equivalent noise bandwidth, and  $D^*$  is the detection.

According to the definition of the SNR of the infrared system, the SNR is determined by the ratio of the irradiance difference at the pupil of the optical system to the equivalent amplitude of the system noise, which is defined as:

$$SNR = \frac{\Delta\Phi}{NEFD} = \frac{V_t}{V_n} \quad (20)$$

where,  $V_t$  is the voltage value of the target signal detected by the system, and  $V_n$  is the RMS value of the infrared detector noise.

Substitute Formulas (17) - (19) into Formula (20), the detection distance of the system is derived as follows:

$$R = \sqrt{\frac{[\mu\Phi(T_t) - \Phi(T_B)] \cdot A_t A_0 \tau_1 D^*}{\sqrt{A'_d \Delta f} (V_n/V_t)}} \quad (21)$$

It can be seen that the detection capability of the infrared radiation system is not only related to the SNR of the system but also affected by other factors including the diffusion coefficient of the target imaging points, the effective area of the infrared detector, the entrance pupil area of the optical system, and the equivalent noise bandwidth. The equivalent noise bandwidth is related to the residence time of the infrared detector. The dispersion phenomenon of the target imaging points is affected by the atmospheric environment, which is directly expressed as the dispersion coefficient of the target imaging in the infrared detector. Therefore, considering the complex and changeable external atmospheric environment, this paper establishes a detection distance calculation model based on the dispersion coefficient. The proposed model provides a certain reference for the infrared system to detect the remote space target.

#### 4. Calculation and analysis

A test platform was used to analyze and verify the rationality and validity of the small target radiation characteristics and detection distance calculation model. The parameters of the infrared camera were as follows. The working band was  $3.7 \mu\text{m} \sim 4.8 \mu\text{m}$ , the number of detector pixels was  $640 \times 512$  pixels, the pixel size was  $15 \mu\text{m} \times 15 \mu\text{m}$ , the output bits were 14, and the focal length was 500 mm. Combined with reference [20, 22], the selected simulation parameters are shown in Table 1.

Table 1. Simulation parameters

Parameter	Value
Temperature/K	298
$\mu$	3
$\Delta f$ /Hz	100
$D^*$ /(Hz <sup>1/2</sup> · W <sup>-1</sup> )	$3 \times 10^9$
$\Phi(T_B)$ /(W · m <sup>-2</sup> · sr <sup>-1</sup> )	$1.45 \times 10^{-5}$
$\tau_1$	0.7319
$A_0$ /m <sup>2</sup>	0.00785

According to Formula (11), the target gray distributions under different target diameters and detection distances are calculated, as shown in Figs. 3-5.

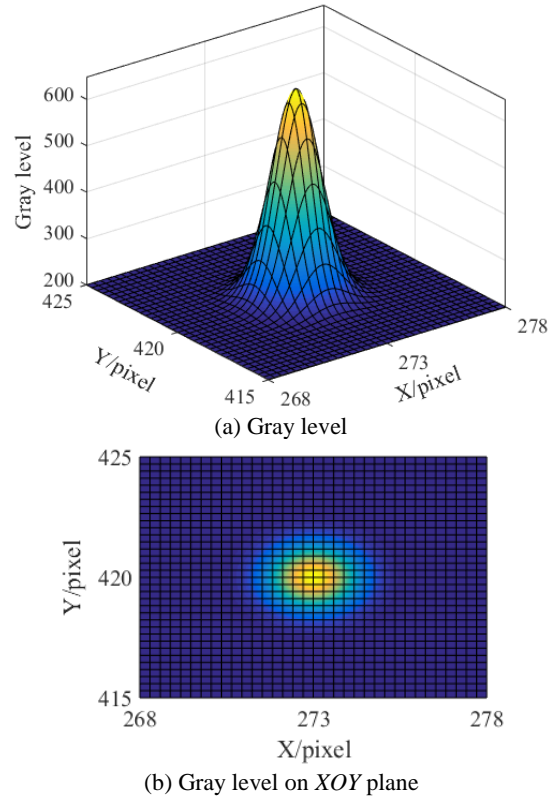


Fig. 3. The gray distribution of the target with a diameter of 100 mm when the detection distance is 800 m (color online)

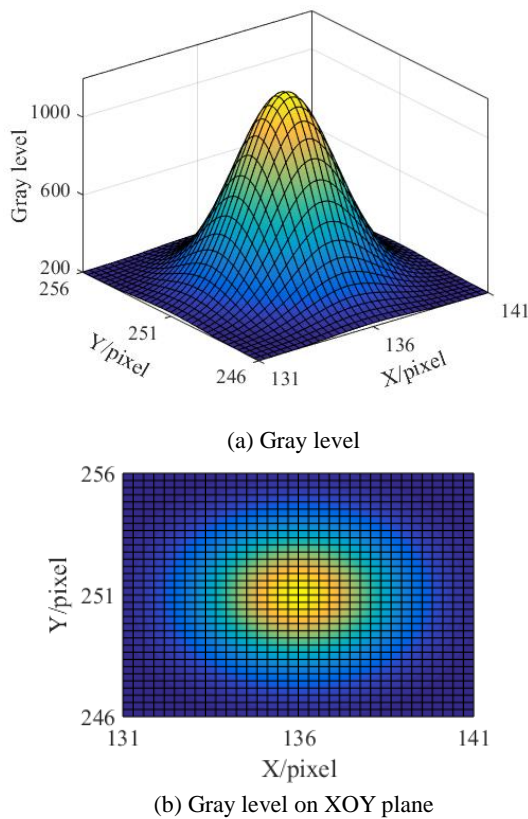


Fig. 4. The gray distribution of the target with a diameter of 200 mm when the detection distance is 800 m (color online)

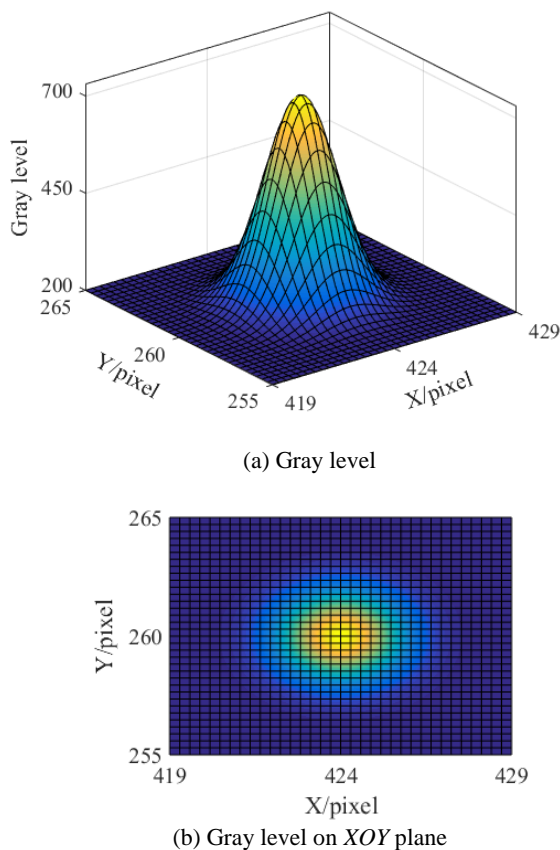


Fig. 5. The gray distribution of the target with a diameter of 200 mm when the detection distance is 1500 m (color online)

Figs. 3 and 4 show the gray distributions of the target with a diameter of 100 mm and 200 mm when the detection distance is 800 m, respectively. When the detection distance is increased to 1500 m, Fig. 5 shows the gray distribution of the target with a diameter of 200 mm. It can be seen that the shapes and gray value distributions of Figs. 3 to 5 are similar. The difference is that even if the detection distance is the same, the location of the target on the imaging surface of the infrared detector changes, because the intersection state of the target and the imaging surface of the system is not completely the same. When the detection distance is the same, the number of pixels occupied by the target imaging increases by four times as the target diameter increases from 100 mm to 200 mm, that is, the target projection area increases by four times. Comparing Figs. 4 and 5, as the detection distance increases from 800 m to 1500 m, not only the target projection area becomes smaller, but also the gray value of the target imaging center becomes smaller.

The gray value of the target imaging and the target projection area affect the target radiation brightness, and the target radiation brightness is also related to the target diameter and the detection distance of the system. According to Formula (13), the relationship between the target radiation brightness and the target diameter under different detection distance conditions is calculated, as shown in Fig. 6.

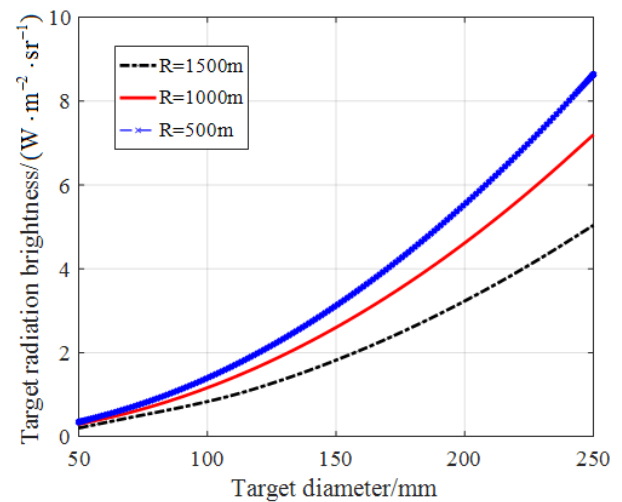


Fig. 6. The relationship between target radiation brightness and target diameter under different detection distances (color online)

It can be seen from Fig. 6 that as the target diameter increases, the number of pixels occupied by the target imaging increases, the target projection area becomes larger, and the target radiation brightness also increases. At the same time, the larger the detection distance of the system is, the slower the increasing trend of the target radiation brightness with the increase of the target diameter is which reflects the nonlinear relationship between the target radiation brightness and the target diameter and detection distance.

Fig. 7 shows the image plane energy distribution of the target under different standard deviation conditions obtained using Formula (14). It can be seen from Fig. 7 that with the increase of the standard deviation value, the image plane energy fluctuation of the target becomes larger, and the energy proportion of the target imaging pixel becomes smaller. At this time, the dispersion of the target imaging is further enhanced.

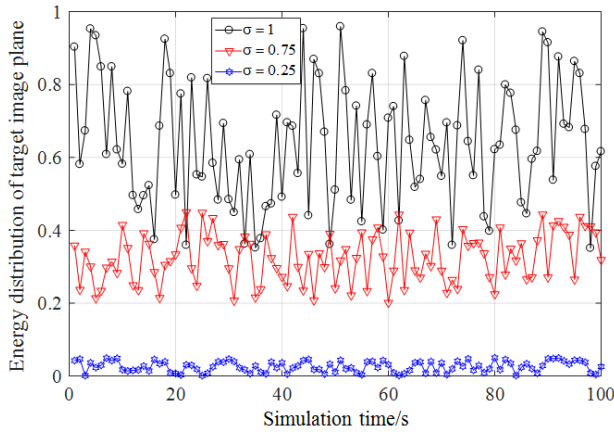
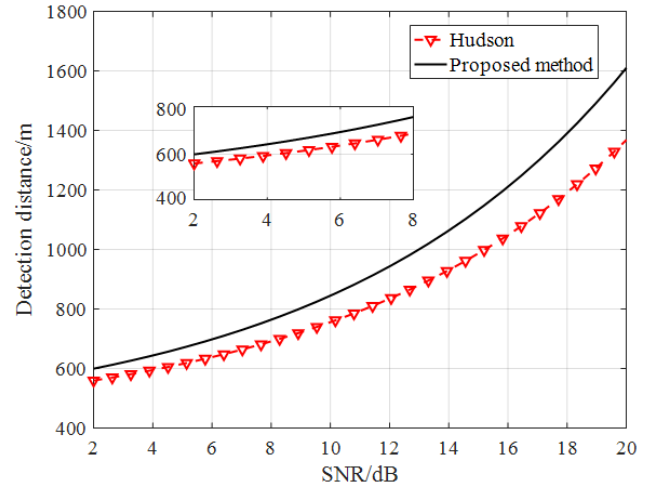


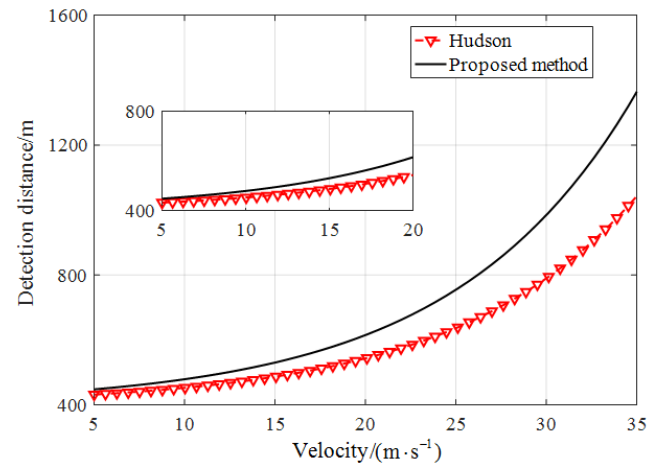
Fig. 7. Image plane energy distribution of target under different standard deviation conditions (color online)

According to Formulas (20) and (21), the traditional Hudson detection distance model [23] and the detection distance model proposed in this paper based on the dispersion coefficient are compared. Fig. 8 shows the relationship between the detection distance of the infrared system varying with the SNR and the target velocity under different models.

It can be seen from Fig. 8 (a) that the changing trend of the detection distance obtained under different models with the SNR is the same, that is, the greater the SNR, the greater the detection distance. When the SNR is less than 8, the detection distances of the two models are similar. When the SNR is greater than 8, the detection distance of the model established in this paper has an obvious trend with the increase in the SNR. It can be seen from Fig. 8 (b) that the trends of the change curves of the detection distance obtained under different models with the target velocity are the same, that is, the faster the flight velocity of the target is, the farther the detection distance is. Since the friction between the airflow and the target surface becomes severe with the increase of the target's flight velocity, this phenomenon increases the heat flow density at the stagnation point of the infrared detector, leading to the enhancement of the target infrared radiation brightness, and improving the detection distance of the system. Furthermore, it can also be seen that the detection distance of the model established by introducing the dispersion coefficient is greater than that of the traditional Hudson method.



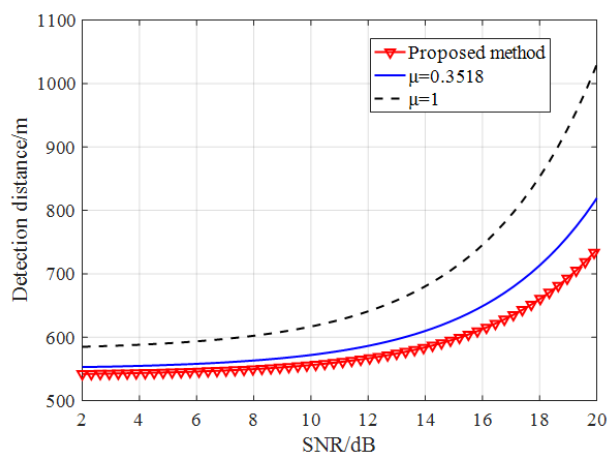
(a) Curves of detection distance changing with the signal-to-noise ratio



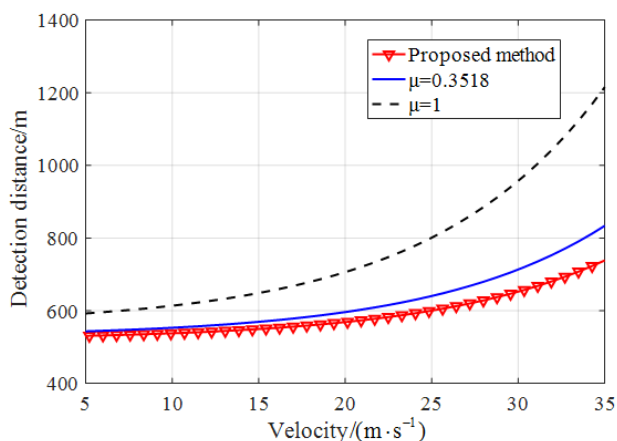
(b) Curves of detection distance changing with the target velocity

Fig. 8. Detection distance variation curves under different models (color online)

Since the dispersion degree of target imaging affects the detection distance of the system, Fig. 9 shows the change curves of detection distance in different dispersion degrees. The three curves in Fig. 9 are the change curve of detection distance established by ignoring the dispersion phenomenon in [24], the fixed dispersion coefficient proposed in [25], and the introduction of the dispersion coefficient in this paper.



(a) Curves of detection distance changing with the signal-to-noise ratio



(b) Curves of detection distance changing with the target velocity

Fig. 9. Detection distance variation curves under different dispersion coefficients (color online)

It can be seen from Fig. 9 that the change curves of the detection distance of the infrared system are not completely the same under different dispersion coefficients. The dispersion phenomenon is not considered in [24], so the dispersion coefficient is 1. In [25], the influence of the dispersion coefficient on the detection distance is considered but with a fixed value of 0.3518. In this paper, the dispersion coefficient is introduced to establish the calculation model of the detection distance, and the detection distance increases with the increase in the dispersion coefficient. The imaging of the target in the infrared detector is affected by the environment. Therefore, it is necessary to consider the dispersion phenomenon. Moreover, the variability of the environment and climate makes the dispersion degree of the target imaging different. Thus, it is more reasonable to determine the dispersion coefficient according to the state of the target and the actual imaging point's dispersion spot.

## 5. Conclusion

According to the principle that the energy of space targets diffuses into multiple pixels and the total energy entering the infrared detector panel remains unchanged, this paper proposes a calculation method for the small target radiation characteristics and detection capability of the infrared radiation system. A test platform with known parameters is utilized to quantitatively analyze the relationship between the target radiation brightness and the target diameter under different detection distance conditions, and the change rule of the detection distance calculation model is established by introducing the dispersion coefficient. The proposed model is compared with the detection distance model based on the traditional Hudson method and the detection distance model with a fixed dispersion coefficient. The comparative results demonstrate that the detection distance model established in this paper changes more slowly with the signal-to-noise ratio and the target velocity, mainly considering the influence of uncertain dispersion phenomenon in the actual test environment, which is more reasonable. The research results in this paper provide a reference for effectively improving the detection performance of the infrared radiation systems for detecting space targets in the complex environment with long range.

## References

- [1] Lihua Cao, Chunming Wan, Yunfeng Zhang, *Journal of Infrared and Millimeter Waves* **34**(4), 460 (2015).
- [2] Hanshan Li, Xiaoqian Zhang, Xuewei Zhang, Quanmin Guo, *Defence Technology* **18**(8), 1405 (2022).
- [3] Sungho Kim, Joohyoung Lee, *Pattern Recognition* **45**(1), 393 (2012).
- [4] Ruiming Liu, Hongliang Zhi, *Journal of Infrared Millimeter and Terahertz Waves* **31**(12), 1491 (2010).
- [5] Hanshan Li, Shiqiang Yue, Xiaoqian Zhang, *Measurement* **186**, 110161 (2021).
- [6] Tieying Qiao, Lihua Cai, Ning Li, Zhou Li, Chenghao Li, *Chinese Optics* **11**(5), 804 (2018).
- [7] Guoqiang Wang, Yuanhao Wu, *Infrared and Laser Engineering* **40**(9), 1634 (2011).
- [8] Chengming Sun, Yan Yuan, Fengzhen Huang, Qian Wang, *Infrared and Laser Engineering* **41**(3), 563 (2012).
- [9] Hongyuan Wang, Yun Chen, *Infrared and Laser Engineering* **45**(5), 19 (2016).
- [10] Jiahao Xie, Shucui Huang, Daozhi Wei, Zhaoyu Zhang, *Acta Optica Sinica* **42**(18), 85 (2022).
- [11] Songtao Chang, Yaoyu Zhang, Zhiyuan Sun, Wei Zhu, *Acta Optica Sinica* **34**(5), 15 (2012).
- [12] Mauricio Delbracio, Pablo Musé, Andrés Almansa, Jean-Michel Morel, *International Journal of Computer Vision* **96**(2), 175 (2012).
- [13] Maojie Luo, Jinmei Zhou, Jingneng Fu, Sheng Liao, *Infrared and Laser Engineering* **42**(1), 36 (2013).
- [14] Ciyin Yang, Lihua Cao, Jianping Zhang, *Optics and*

- Precision Engineering **22**(7), 1751 (2014).
- [15] Guoqing Yang, Zhou Li, Chen Zhao, Yi Yu, Yanfeng Qiao, Fengyun He, *Infrared and Laser Engineering* **49**(5), 185 (2020).
- [16] Weiwei Xu, Liming Zhang, Benyong Yang, Yanli Qiao, *Acta Optica Sinica* **32**(2), 164 (2012).
- [17] Hailong Chen, Ao Zhang, Xuemei Liu, Jing Li, Shaoguang Li, *Acta Optica Sinica* **41**(21), 164 (2021).
- [18] Pascasie L. Dombert, Anna Kuhns, Paola Mengotti, Gereon R. Fink, Simone Vossel, *NeuroImage* **142**, 553 (2016).
- [19] Hanshan Li, Xiaoqian Zhang, *Defence Technology* **18**(9), 1643 (2022).
- [20] Ni Li, Zhenhua Lv, Wenqin Huai, Guanghong Gong, *Infrared Physics and Technology* **77**, 153 (2016).
- [21] Hanshan Li, Xiaoqian Zhang, Xuwei Zhang, Junchai Gao, *IEEE Sensors Journal* **21**(21), 24001 (2021).
- [22] Taimur Rashid, Hassan A. Khawaja, K. Edvardsen, Umair N. Mughal, *Sensors and Transducers* **194**(11), 62 (2015).
- [23] Shiyu Cao, Guixiang Li, Zhihuai Li, Lifeng Yan, *Journal of Air Force Radar Academy* **25**(5), 318 (2011).
- [24] Xia Mao, Le Chang, Weihe Diao, *Journal of Beijing University of Aeronautics and Astronautics* **37**(11), 1429 (2011).
- [25] Yang Zhang, Guangya Shi, Yanzheng Wang, *Systems Engineering and Electronics* **42**(7), 1510 (2020).

---

\*Corresponding author: linli202288@yeah.net